

HETEROCYCLES, Vol. 80, No. 1, 2010, pp. 527 - 535. © The Japan Institute of Heterocyclic Chemistry
Received, 22nd July, 2009, Accepted, 31st August, 2009, Published online, 1st September, 2009
DOI: 10.3987/COM-09-S(S)64

PREPARATION AND FERROELECTRIC PROPERTIES OF NEW CHIRAL LIQUID CRYSTALLINE ORGANIC RADICAL COMPOUNDS

Naohiko Ikuma,¹ Katsuaki Suzuki,¹ Yoshiaki Uchida,¹ Rui Tamura,^{*1}
Yoshio Aoki,² and Hiroyuki Nohira²

¹Graduate School of Human and Environmental Studies, Kyoto University,
Kyoto 606-8501, Japan

²Graduate School of Science and Engineering, Saitama University, Saitama,
338-8570, Japan

email: tamura-r@mbox.kudpc.kyoto-u.ac.jp

Abstract – We have synthesized new chiral liquid crystalline (LC) organic radical compounds **2** and **3**, which are the derivatives of the previously reported compounds **1** containing a chiral cyclic nitroxide unit and an ester group in the mesogen core, and their ferroelectric properties have been studied. The enantiomerically enriched (2*S*,5*S*)-**2** and (2*S*,5*S*)-**3** showed an SmC* phase for which their ferroelectric properties such as spontaneous polarization (*P*_s) and tilt angle (θ) were compared with those of (2*S*,5*S*)-**1**.

INTRODUCTION

Recently, we have shown that a 2,2,5,5-tetrasubstituted pyrrolidin-1-yloxy (PROXYL) structure is stable enough for repeated heating and cooling cycles below 150°C in the air and thereby this radical unit can serve as the excellent source of the magnetic spin ($S = 1/2$) and spontaneous polarization (*P*_s) for elaborating paramagnetic as well as ferroelectric all-organic liquid crystals (LCs), which can combine the optical and electric properties of conventional ferroelectric LCs (FLCs) with the magnetic properties of paramagnetic compounds.¹⁻⁹ For example, it is quite interesting to know whether magneto-electric effects can be observed in the FLC state of paramagnetic materials. The magneto-electric effects are well known to arise from the intra- and intermolecular interactions between magnetic and electric dipole moments and to be observed in ferroelectric rare earth metal manganite crystals such as YMnO₃, TbMnO₃, and

HoMnO₃ with magnetic order at low temperatures.¹⁰⁻¹² Experimentally, the effects can be detected as the influence of a magnetic (electric) field on the polarization (magnetization) of a material and *vice versa*.¹³⁻¹⁵

In this context, we successfully obtained the prototypic all-organic chiral LC radical compounds **1** which have a PROXYL group with a large electric dipole moments (3 Debye) in the mesogen core as well as a polar ester group (1.8 Debye) used very often for the preparation of conventional FLCs.¹⁶ Indeed, (2*S*,5*S*)-**1** (n=11–15) showing an SmC* phase exhibited ferroelectricity in a thin sandwich cell (4 μm thickness); the highest *P_s* value of 24 nC cm⁻² was recorded for (2*S*,5*S*)-**1** (n=13).^{2,3}

In order to improve the *P_s* value which should become a crucial factor for observing magneto-electric effects in the paramagnetic FLCs, we have designed compounds (2*S*,5*S*)-**2** and (2*S*,5*S*)-**3** with an additional benzene ring on either 2 or 5 position of the PROXYL ring, compared to (2*S*,5*S*)-**1** (Chart 1). This structural modification is expected to result in the strong intra-layer interactions in the SmC* phase and hence to increase the overall *P_s* value.¹⁷ Here we report the synthesis, LC characterization and ferroelectric properties of (2*S*,5*S*)-**2** and (2*S*,5*S*)-**3**.

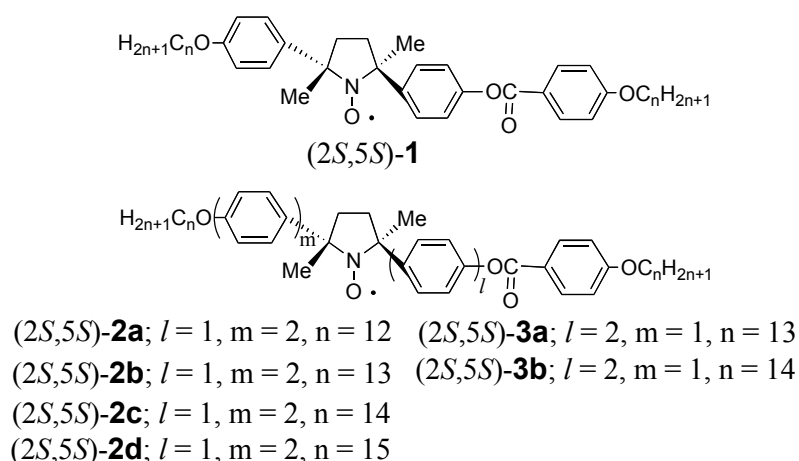
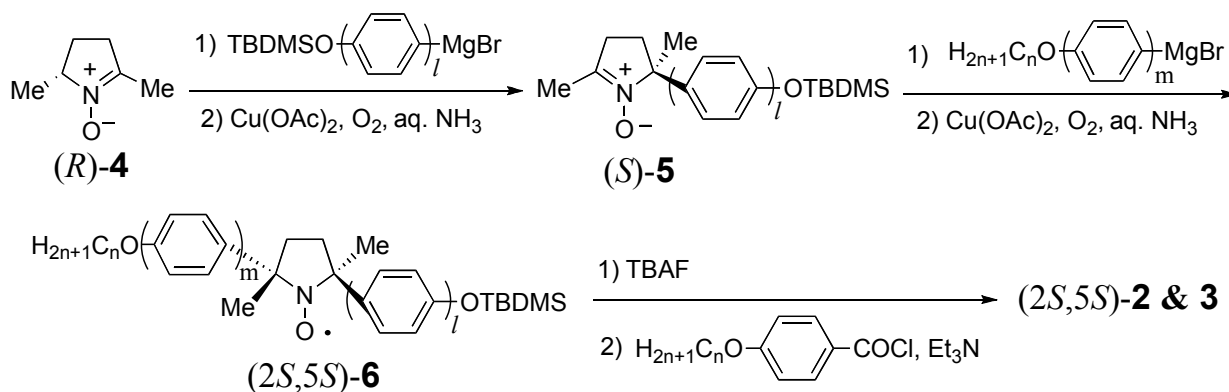


Chart 1. PROXYL type of LC compounds (2*S*,5*S*)-**1–3** showing an SmC* phase.



Scheme 1. Preparation of (2*S*,5*S*)-**2** and (2*S*,5*S*)-**3**.

RESULTS AND DISCUSSION

Synthesis of (2S,5S)-2 and (2S,5S)-3. (2S,5S)-2 and (2S,5S)-3 were synthesized with high stereoselectivity by repeating the addition of an appropriate Grignard reagent to nitrones [4 (*ca.* 90% *ee*) and 5] and the subsequent oxidation twice, followed by benzylation of the phenolic hydroxy group after desilylation, similarly to the synthesis of (2S,5S)-1 (Scheme 1).^{1-3,18-23}

Characterization of LC phases. The phase transition behavior of (2S,5S)-2 and (2S,5S)-3 was characterized by DSC, POM, and XRD analyses, which were measured below 160°C because these compounds instantly decompose in the isotropic phase above 160°C (Table 1, Figure 1 and 2).

Table 1. Phase transition temperatures of (2S,5S)-2 and (2S,5S)-3 on the first heating run.

(2S,5S)-2 or 3	<i>ee</i> (%)	Transition temperature (°C) and ΔH (in parentheses, kJ/mol)						
		Cr	SmC*	N*	I			
2a (n=12)	89.3	•	105.9 (30.6)	•	129.7 (0.4)	•	163.8 (2.2)	•
2b (n=13)	91.0	•	105.5 (33.2)	•	150.1 (1.2)	•	167.4 (2.2)	•
2c (n=14)	90.9	•	106.5 (36.9)	•	154.9 (1.7)	•	164.8 (3.3)	•
2d (n=15)	90.8	•	106.2 (38.1)	•	155.0 (7.1) ^a	•	159.8 (7.1) ^a	•
3a (n=13)	91.2	•	105.6 (22.8)	•	154.4 (2.1)	•	165.2 (2.0)	•
3b (n=14)	89.0	•	107.2 (37.3)	•	159.7 (8.6) ^a	•	164.5 (8.6) ^a	•

^a Two peaks were overlapped.

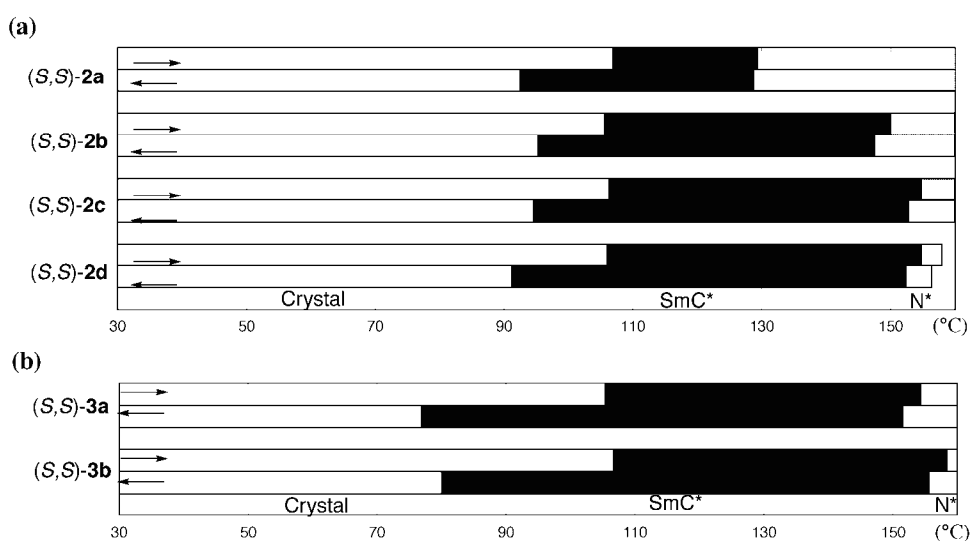


Figure 1. LC behavior of (a) (2S,5S)-2 and (b) (2S,5S)-3. Transition temperatures determined by DSC analysis at a scanning rate of 5°C min⁻¹ upon the first heating and cooling processes. Heating was turned down at 160°C for the subsequent cooling run.

As expected, (2*S*,5*S*)-**2** and (2*S*,5*S*)-**3** showed stable LC phases over wide temperature ranges and at higher temperatures than (2*S*,5*S*)-**1** due most likely to the stronger inter-layer interactions.¹⁷ Similarly to the case of (2*S*,5*S*)-**1**, (2*S*,5*S*)-**2** with C12 to C15 chains and (2*S*,5*S*)-**3** with C13 and C14 chains exhibited SmC* and N* phases, with respective broken fan-shaped and oily-streak textures observed on the cooling run (Table 1, Figure 1 and 2). Variable temperature XRD analysis verified the existence of the SmC* and N* phases (Figure 3).

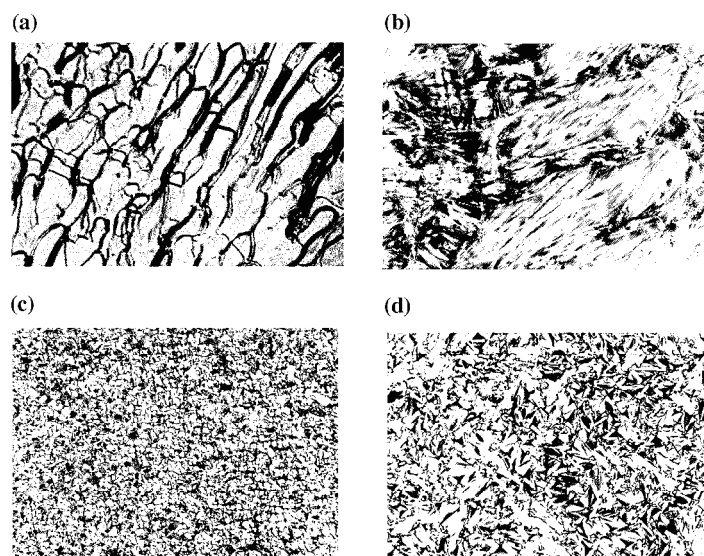


Figure 2. Polarized optical micrographs showing (a) oily-streaks texture (N*) under random conditions at 158°C and (b) broken fan-shaped texture (SmC*) in a thin sandwich cell (4 mm) under homogeneous planar boundary conditions at 130°C for (2*S*,5*S*)-**2b**, and (c) oily-streaks texture (N*) under random conditions at 160°C and (d) broken fan-shaped texture (SmC*) in a thin sandwich cell (4 μm) under homogeneous planar boundary conditions at 150°C for (2*S*,5*S*)-**3b**.

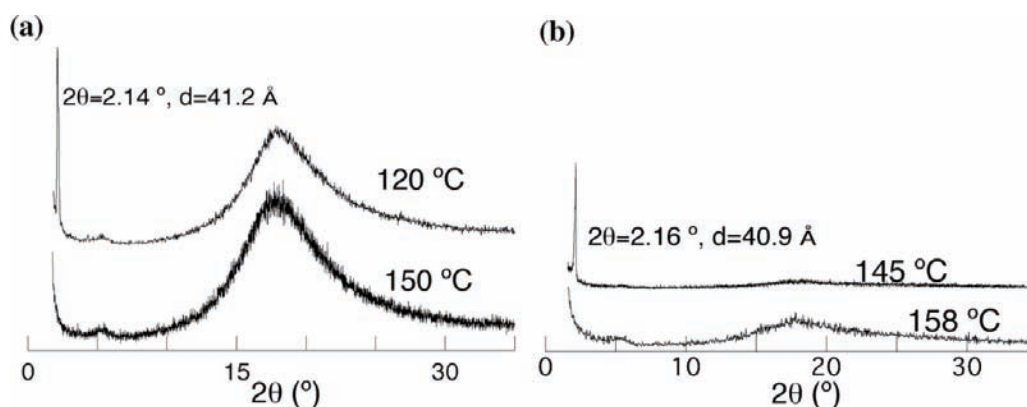


Figure 3. XRD patterns of (a) (2*S*,5*S*)-**2a** at 120 (SmC*) and 150°C (N*) and (b) (2*S*,5*S*)-**3a** at 145 (SmC*) and 158°C (N*).

Ferroelectric properties. The magnitude of P_s and the optical and calculated tilt angles [θ and $\cos^{-1}(d/l)$] of (2*S*,5*S*)-**2** and (2*S*,5*S*)-**3** are summarized in Figures 4 and 5 and Table 2. On the cooling run from the N*-to-SmC* transition temperature, the P_s values rapidly increased (Figure 4). On the whole, the P_s values of (2*S*,5*S*)-**2** were larger than those of the corresponding (2*S*,5*S*)-**1** and (2*S*,5*S*)-**3**; (2*S*,5*S*)-**2d** showed the highest $P_s(-10^\circ)$ value of 32 nC cm⁻² (Figure 4a and Table 2). Such high P_s values observed for (2*S*,5*S*)-**2** can be interpreted in terms of the increased intra-layer interactions.¹⁷ The tilt angles of (2*S*,5*S*)-**2** and (2*S*,5*S*)-**3** were too large to measure the optical response time (Figure 5 and Table 2); only a bright-dark-bright or dark-bright-dark texture change was observed upon switching the polarity of the applied electric field.

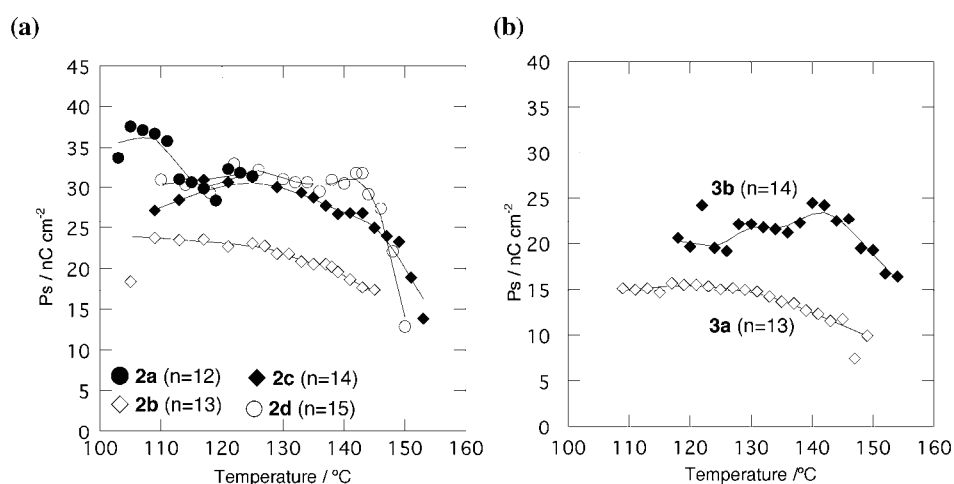


Figure 4. Temperature dependence of the P_s value in the SmC* phases of (a) (2*S*,5*S*)-**2** and (b) (2*S*,5*S*)-**3**.

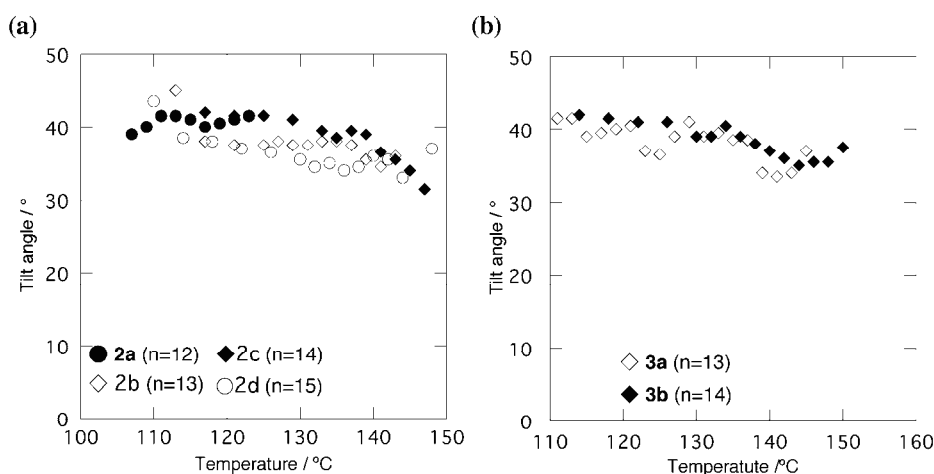


Figure 5. Temperature-dependence of the tilt angle (θ) of (a) (2*S*,5*S*)-**2** and (b) (2*S*,5*S*)-**3** measured by hot-stage POM.

Moreover, in contrast to the case of (2*S*,5*S*)-**1**, we observed the relaxation of the ferroelectric state of (2*S*,5*S*)-**2a** and (2*S*,5*S*)-**2b** in the same type of FLC cell, i.e., POM texture change by turning off the

electric fields (Figure 6). At the same time, the textures in the two field-free states of (2*S*,5*S*)-**2a** or (2*S*,5*S*)-**2b** considerably differed from each other, suggesting the short-pitch SmC* nature and the incomplete formation of a helical superstructure in the FLC cell used (Figures 6b and d).

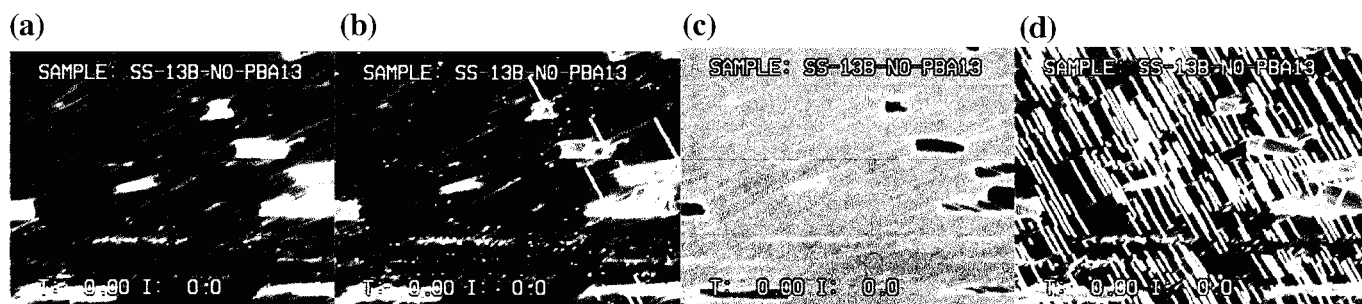


Figure 6. Ferroelectric switching modes of (2*S*,5*S*)-**2b** in a sandwich cell (4 μm) at 130°C under homogeneous planar boundary conditions between crossed polarizers. Applied DC voltage dependence of texture change in the same area at 110°C: Electric field sweeping in the order of (a) +12 V, (b) 0 V, (c) -12 V, and (d) 0V.

Table 2. Ferroelectric properties measured in the SmC* phases of (2*S*,5*S*)-**2** and (2*S*,5*S*)-**3**, layer distances, calculated molecular length, and geometrical tilt angles.

Compound	$P_s(-10^\circ)^{a,b}$ [nC cm ⁻²]	$\theta(-10^\circ)^{b,c}$ [deg]	d^d [Å]	l^e [Å]	$\cos^{-1}(d/l)^f$ [deg]
2a (n=12)	28 (119°C)	41	41.2 (120°C)	50.6	35
2b (n=13)	21 (137°C)	38	40.3 (120°C)	53.1	41
2c (n=14)	27 (143°C)	36	41.5 (120°C)	54.8	41
2d (n=15)	32 (142°C)	36	43.7 (130°C)	57.4	40
3a (n=13)	12 (141°C)	34	40.9 (145°C)	55.4	42
3b (n=14)	23 (146°C)	36	42.6 (145°C)	57.7	42

^aSpontaneous polarization. ^bMeasured at a temperature 10°C below the phase transition from the N* phase to the SmC* phase during the cooling process. ^cTilt angle measured by hot-stage POM. ^dLayer distance from XRD data. ^eMolecular length determined by a PM3 semiempirical calculation (PC Spartan'02). ^fCalculated geometrical tilt angle from d and l values.

In summary, we could obtain new chiral organic radical compounds with strong inter-layer interactions which showed FLC properties at high temperatures and over wide temperature ranges. Above all, (2*S*,5*S*)-**2d** showed the highest $P_s(-10^\circ)$ value of 32 nC cm⁻², which was larger than that (24 nC cm⁻²) of (2*S*,5*S*)-**1** (n=13) previously reported.^{2,3}

EXPERIMENTAL

General. Transition temperatures refer to the peak top of each transition curve by DSC analysis, which was performed at a scanning rate of $5\text{ }^{\circ}\text{C min}^{-1}$. Enantiomeric excess (*ee*) were determined by HPLC analysis using a chiral stationary phase column (Daicel Chiralpak AD, $0.46 \times 25\text{ cm}$), a mixture of hexane and 2-PrOH (9:1) as the mobile phase at a flow rate of 1.0 mL min^{-1} , and a UV-vis spectrometer (254 nm) as the detector. *Ps* was measured by the triangular wave method at a frequency of 20 Hz in a thin sandwich cell (EHC Co., Japan; thickness of $4\text{ }\mu\text{m}$) coated with ITO electrodes and covered with antiparallel-rubbed polyimide films in an electric field of 10 V peak to peak. Tilt angles were measured by polarized optical microscopy (POM). Their *g* values and hyperfine coupling constants (a_{N}) were determined by electron paramagnetic resonance (EPR) spectroscopy in THF at $25\text{ }^{\circ}\text{C}$. The variable temperature X-ray diffraction (XRD) patterns were recorded at a continuous scanning rate of $2^{\circ} 2\theta\text{ min}^{-1}$ at a heating and cooling rate of $4\text{ }^{\circ}\text{C min}^{-1}$ using $\text{CuK}\alpha$ radiation (40 kV, 20 mA), with the intensity of the diffracted X-rays being collected at intervals of $0.02^{\circ} 2\theta$.

General synthetic procedure for (2S,5S)-2 and (2S,5S)-3. Enantiomerically enriched nitron (*R*)-4 (ca. 90% *ee*) was prepared according to the published procedure.^{18,19} The nitron (*R*)-4 (0.452 g, 4.0 mmol) was reacted with the first Grignard reagent (8.0 mmol) in THF (5 mL) at $-78\text{ }^{\circ}\text{C}$. The reaction temperature was slowly raised to $25\text{ }^{\circ}\text{C}$. After being stirred overnight, the reaction mixture was poured into saturated aqueous NH_4Cl solution (50 mL), followed by extraction with CH_2Cl_2 (2 x 50 mL) and concentration in vacuo. The residue was dissolved in MeOH (20 mL) and oxidized by treatment with $\text{Cu}(\text{OAc})_2 \cdot \text{H}_2\text{O}$ (0.13 g), conc. NH_3 solution (1.1 mL), and O_2 bubbling until dark blue color developed in solution. The solution was evaporated in vacuo, and the residue extracted by CHCl_3 (50 mL). The organic phase was washed with saturated aqueous NaHCO_3 solution (50 mL), dried over MgSO_4 , and concentrated in vacuo to give the crude nitron (*S*)-5. The crude (*S*)-5 was reacted with the second Grignard reagent (8.0 mmol) and the resulting crude addition product was oxidized by the same procedure. The crude (*2S,5S*)-6 was roughly purified by column chromatography on silica gel (hexane: CH_2Cl_2 : Et_2O 6/4/0~6/3/1) to remove mainly the less polar impurities. Then to this crude (*2S,5S*)-6 dissolved in THF (20 mL) was added a THF solution of Bu_4NF (1 M solution, 1.0 mL) at $0\text{ }^{\circ}\text{C}$. After being stirred at $0\text{ }^{\circ}\text{C}$ for 20 min, the reaction mixture was poured into saturated aqueous NH_4Cl solution (30 mL), followed by extraction with CH_2Cl_2 (2 x 50 mL), drying over MgSO_4 , and concentration in vacuo. The crude product was purified by column chromatography on silica gel (hexane: CH_2Cl_2 : Et_2O 6/3/1~5/3/2) to give the pure desilylated product of (*2S,5S*)-6 as yellow solid in ca. 10% yield from (*R*)-4.

To a mixture of the desilylated product (0.3 mmol) and Et₃N (0.9 mL) in THF (10 mL) was added an appropriate *p*-alkoxybenzoyl chloride (0.9 mmol) in THF (3 mL) at 0°C. The reaction mixture was slowly warmed to 25 °C and stirred for 40 h. Then the mixture was poured into a saturated aqueous NaHCO₃ solution (20 mL) and the aqueous mixture was extracted with Et₂O (2 x 50 mL). The combined organic phase was dried over MgSO₄ and evaporated in vacuo. Column chromatography on silica gel (hexane:CH₂Cl₂:Et₂O 8/2/0~7/2/1) of the residue gave pure (2*S*,5*S*)-**2** or (2*S*,5*S*)-**3** as yellow solid in 70-80% yield from (2*S*,5*S*)-**6**.

(2*S*,5*S*)-**2a**: [α]_D²⁴ -71.49 (89.3% *ee*, c 1.001, THF). EPR (THF): *g* = 2.0057, *a*_N = 1.33 mT. IR (KBr): 2923, 2850, 1734, 1607, 1507, 1395, 1254, 1164, 1071, 813, 764. Anal. Calcd for C₅₅H₇₇NO₅: C, 79.47; H, 9.22; N, 1.69. Found: C, 79.39; H, 9.44; N, 1.70.

(2*S*,5*S*)-**2b**: [α]_D²⁵ -72.91 (91.0% *ee*, c 0.982, THF). EPR (THF): *g* = 2.0060, *a*_N = 1.34 mT. IR (KBr): 2849, 1735, 1604, 1507, 1395, 1250, 1164, 1078, 820, 765. Anal. Calcd for C₅₇H₈₁NO₅: C, 79.68; H, 9.38; N, 1.63. Found: C, 79.69; H, 9.41; N, 1.60.

(2*S*,5*S*)-**2c**: [α]_D²⁵ -70.40 (90.9% *ee*, c 0.991, THF). EPR (THF): *g* = 2.0058, *a*_N = 1.33 mT. IR (KBr): 2915, 1731, 1607, 1498, 1371, 1254, 1201, 1165, 1077, 819, 764. Anal. Calcd for C₅₉H₈₅NO₅: C, 79.86; H, 9.54; N, 1.58. Found: C, 79.90; H, 9.60; N, 1.55.

(2*S*,5*S*)-**2d**: [α]_D²⁵ -67.13 (90.8% *ee*, c 0.984, THF). EPR (THF): *g* = 2.0059, *a*_N = 1.33 mT. IR (KBr): 2922, 2851, 1730, 1606, 1511, 1371, 1254, 1201, 1164, 1977, 823, 764. Anal. Calcd for C₆₁H₈₉NO₅: C, 80.04; H, 9.69; N, 1.53. Found: C, 80.23; H, 9.52; N, 1.57.

(2*S*,5*S*)-**3a**: [α]_D²⁵ -71.27 (91.2% *ee*, c 1.006, THF). EPR (THF): *g* = 2.0055, *a*_N = 1.33 mT. IR (KBr): 2917, 2853, 1731, 1605, 1509, 1372, 1256, 1206, 1169, 1079, 850, 767. Anal. Calcd for C₅₇H₈₁NO₅: C, 79.68; H, 9.38; N, 1.63. Found: C, 79.44; H, 9.39; N, 1.65.

(2*S*,5*S*)-**3b**: [α]_D²⁵ -67.84 (89.0% *ee*, c 1.003, THF). EPR (THF): *g* = 2.0056, *a*_N = 1.32 mT. IR (KBr): 2921, 2851, 1730, 1605, 1510, 1372, 1255, 1206, 1169, 1079, 876, 767. Anal. Calcd for C₅₉H₈₅NO₅: C, 79.86; H, 9.54; N, 1.58. Found: C, 79.76; H, 9.53; N, 1.63.

REFERENCES AND NOTES

1. N. Ikuma, R. Tamura, S. Shimono, N. Kawame, O. Tamada, N. Sakai, J. Yamauchi, and Y. Yamamoto, *Angew. Chem. Int. Ed.*, 2004, **43**, 3677.
2. N. Ikuma, R. Tamura, S. Shimono, Y. Uchida, K. Masaki, J. Yamauchi, Y. Aoki, and H. Nohira, *Adv. Mater.*, 2006, **18**, 477.

3. N. Ikuma, R. Tamura, S. Shimono, K. Masaki, Y. Uchida, J. Yamauchi, Y. Aoki, and H. Nohira, *Ferroelectrics*, 2006, **343**, 119.
4. Y. Uchida, R. Tamura, N. Ikuma, J. Yamauchi, Y. Aoki, and H. Nohira, *Mol. Cryst. Liq. Cryst.*, 2007, **479**, 213.
5. Y. Uchida, R. Tamura, N. Ikuma, J. Yamauchi, Y. Aoki, and H. Nohira, *Ferroelectrics*, 2008, **365**, 158.
6. Y. Uchida, N. Ikuma, R. Tamura, S. Shimono, Y. Noda, J. Yamauchi, Y. Aoki, and H. Nohira, *J. Mater. Chem.*, 2008, **18**, 2950.
7. R. Tamura, N. Ikuma, and Y. Uchida, *J. Mater. Chem.*, 2008, **18**, 2872.
8. G. I. Likhtenshtein, J. Yamauchi, S. Nakatsuji, A. I. Smirnov, and R. Tamura, 'Nitroxides: Applications in Chemistry, Biomedicine, and Materials Science,' Wiley-VCH, Weinheim, 2008.
9. R. Tamura, N. Ikuma, and S. Shimono, In 'Soft Nanomaterials, Vol. 1,' ed. by H. S. Nalwa, American Scientific Publishers, California, 2009, pp. 257-277.
10. M. Fiebig, T. Lottermoser, D. Fröhlich, A.V. Goltsev, and R. V. Pisarev, *Nature*, 2002, **419**, 818.
11. T. Kimura, T. Got, G. Shintani, K. Ishizuka, T. Arima, and Y. Tokura, *Nature*, 2003, **426**, 55.
12. T. Lottermoser, T. Lonkai, U. Amann, D. Hohlwein, J. Ihringer, and M. Fiebig, *Nature*, 2004, **430**, 541.
13. C. Falser, G. H. Fecher, and B. Balke, *Angew. Chem. Int. Ed.*, 2007, **46**, 668.
14. C. N. Rao and C. R. Serrano, *J. Mater. Chem.*, 2007, **17**, 4931.
15. W. Erenstein, N. D. Mathur, and J. F. Scott, *Nature*, 2006, **442**, 759.
16. D. M. Walba, *Top. Stereochem.*, 2003, **24**, 457.
17. V. Bezborodov, V. Lapanik, G. Sasnouski, and W. Haase, *Ferroelectrics*, 2006, **343**, 49.
18. J. Einhorn, C. Einhorn, F. Ratajczak, I. Gautier-Lunear, and J.-L. Pierre, *J. Org. Chem.*, 1997, **62**, 9385.
19. R. P. Short, R. M. Kennedy, and S. Masamune, *J. Org. Chem.*, 1989, **54**, 1755.
20. N. Benfaremo, M. Steenbock, M. Klapper, K. Müller, V. Enkelmann, and K. Cabrera, *Liebigs Ann. Chem.*, 1996, 1413.
21. N. Ikuma, R. Tamura, S. Shimono, N. Kawame, O. Tamada, N. Sakai, J. Yamauchi, and Y. Yamamoto, *Mendeleev Commun.*, 2003, 109.
22. N. Ikuma, R. Tamura, S. Shimono, N. Kawame, O. Tamada, N. Sakai, Y. Yamamoto, and J. Yamauchi, *Mol. Cryst. Liq. Cryst.*, 2005, **440**, 23.
23. N. Ikuma, H. Tsue, N. Tsue, S. Shimono, Y. Uchida, K. Masaki, N. Matsuoka, and R. Tamura, *Org. Lett.*, 2005, **7**, 1797.